# Supplementary material - Nonlocal effects dominate the global mean surface temperature response to the biogeophysical effects of deforestation

Johannes Winckler[1,2,3] *, Quentin Lejeune[4,5], Christian H. Reick[1], Julia Pongratz[1,6]

[1]Max Planck Institute for Meteorology, 20146 Hamburg, Germany.

[2]International Max Planck Research School on Earth System Modeling, 20146 Hamburg, Germany.

[3]Current affiliation: Laboratoire des Sciences du Climat et de l'Environnement, LSCE/IPSL, CEA-CNRS-UVSQ, Université Paris-Saclay, 91191 Gif-sur-Yvette, France.

[4]Institute for Atmospheric and Climate Science, ETH-Zürich, 8092 Zurich, Switzerland.

[5] Current affiliation: Climate Analytics, 10969 Berlin, Germany.

[6] Current affiliation: Ludwig-Maximilians-Universität München, 80333 Munich, Germany

*e-mail: johannes.winckler@mpimet.mpg.de

This manuscript was compiled on December 15, 2018

## Contents of this file

## Introduction

This supplement provides additional information for the paper 'Nonlocal effects dominate the global mean surface temperature response to the biogeophysical effects of deforestation'. The figures are numbered according to the order of their reference in the main text.

- Text S1 explains the moving-window approach that is applied to separate local and nonlocal effects on surface temperature in various climate models.

- Text S2 provides details on the observation-based datasets that are used in Fig 1 in the main text.

- Text S3 explains how the warming due to deforestation-induced land carbon losses (gray bar in Fig. 2b in the main text) is estimated.

- Fig. S1 shows the changes in radiometric surface temperature due to the local effects of deforestation in four observation-based datasets (Methods). These maps correspond to the latitudinal averages in Fig. 1 in the main text.

- Fig. S2 shows the vegetated fraction that was used in the idealized simulations in the MPI-ESM.

- Fig. S3 shows the maps of the local and nonlocal effects on surface temperature for a selection of the global mean values shown in Fig. 2 in the main text.

- Fig. S4 shows the maps of the local and nonlocal effects on surface temperature in the simulation '3/4' for the DJF and JJA seasons separately.

- In Fig. S5, the nonlocal effects of deforestation on surface temperature are shown for deforestation in broad latitudinal bands. The maps correspond to the global mean values shown in Fig. 2*b* in the main text.

- In Fig. S6, the mechanisms underlying nonlocal effects on surface temperature are analyzed separately for deforestation and changes in surface albedo. Shown are changes in surface incoming radiation, split up into shortwave and longwave incoming radiation.

- In Fig. S7, the mechanisms underlying local effects on surface temperature are analyzed separately for deforestation and changes in surface albedo. To this end, we decompose changes in the surface energy balance into changes in net available energy and changes in turbulent heat fluxes.

- Fig. S8 compares the the two different methods used in this thesis for calculating the local effects on surface temperature in plausible LCC scenarios.

- Fig. S9 provides maps of the simulated local plus nonlocal effects for all idealized experiments in the MPI-ESM and indicates where these results are statistically significant.

- Table S1 provides an overview over the simulations in the MPI-ESM.

- Table S2 provides an overview over the simulations used in Fig. 3 in the main text.

## Text S1 - Moving-window approach to separate local and nonlocal effects in various climate models

For separating local and nonlocal effects from existing climate model simulations, we employ the moving window approach as in the paper by Lejeune et al.[1] In this approach, linear regressions are fitted between the simulated temporal changes in surface temperature and those in tree fraction within spatially moving windows, each of which contains 5 x 5 model grid cells. For the grid cell located in the center of each moving window, the local effects of deforestation on surface temperature are then computed by multiplying the slope of the regression by the actual temporal change in tree fraction over this particular grid cell. This approach assumes that the forcing that is induced by deforestation acts spatially heterogeneously and thus mostly affects surface temperature in each grid cell separately, as opposed to greenhouse gases and other climate forcings which impact surface temperature similarly for all grid cells within one moving window. An evaluation of this method as well as further details are available in their study.[1]

For this particular set of existing simulations (historical, RCP2.6 and RCP8.5, see Table S2), we then calculate the nonlocal effects as the simulated total minus local effects, which is different from the approach for the idealized simulations in the MPI-ESM (Methods in main text) where we first isolated the nonlocal effects and then used them for obtaining the local effects. We use the last 30 years in which data are available for all models. These years are 1971 - 2000 for historical changes in forest cover, and 2070 - 2099 for changes in forest cover in the RCP simulations. Different numbers of ensemble members are available for the different models. For instance, for RCP2.6 in the MPI-ESM, there are 3 ensemble members with and 2 without deforestation. Thus, in Fig. 3 in the main text we show $3 \times 2 = 6$ combinations of ensemble members. For the numbers of available ensemble members in the respective models, see Table S2.

## Text S2 - Details on the observation-based datasets

The observation-based datasets should be compared with care because they differ in many respects. For instance because the spatial coverage (coloured areas in Fig. S1) and the underlying methods differ strongly. In addition, while the three satellite-based datasets[2–4] only employ observations under cloud-free conditions, the ground-based observations[5] are free of this cloud bias. Furthermore, conversions between different vegetation types are analyzed in the different datasets. The dataset by Li et al.[2] considers differences between forests and 'open land' (grasslands and croplands). The dataset by Alkama et al.[3] considers forest loss related to disturbances such as forest fires or windstorms, but also forest clearings for agriculture or forestry. The dataset by Bright et al.[5] includes the effects of a conversion between different forest types and grass. We average their responses to the replacement of different forest types by grass (their Figs. 2 $d$, $e$, $f$), and we weigh this average with the occurrence of the respective forest type in the MPI-ESM. The dataset by Duveiller et al.[4] contains information on the local effects of conversions between various land covers. Here, we consider the conversion of forests to crops and grasslands (variable '13' in their datasets 'LSTday_IGBPgen.nc' and 'LSTnight_IGBPgen.nc') and average daytime and nighttime values. Finally, the datasets differ in the years over which they average their local effects of potential deforestation (Li et al. 2002-2013; Alkama et al. 2003-2012; Bright et al. 2001-2011; Duveiller et al. 2000-2015). Because the local effects exclude a large share of climate variability[6] we assume that the multi-year averages of the observations are robust with respect to the exact number of years over which the average is calculated, and thus the multi-year average can be compared consistently to the 200-year average in the MPI-ESM.

For the observational range in Fig. 1 in the main text, we average latitudinally over locations where values in at least one of the four datasets are available. For the dataset by Alkama et al.,[3] we weighted the data for the latitudinal average with the forest loss at the respective locations. The corresponding Fig. S1 shows only locations where forest loss exceeds 1% in the analysis time frame (years 2003 - 2012).

## Text S3 - Deforestation-induced warming due to land carbon loss

To provide a first-order estimate of the importance of biogeophysical effects to those of deforestation–related carbon emissions we estimate how much carbon would be released to the atmosphere by the deforestation applied in the '2x_historical' simulation. For this, we scale the respective deforestation areas with carbon values of different forest types as used in a bookkeeping model for land-use emissions.[7] The range in Fig. 2 includes an upper estimate (starting with values for primary forest of the default dataset used in that study) and a lower estimate (starting with values for secondary forest of the alternative dataset with lower carbon values). The resulting change in carbon is then converted in a change into global mean temperature (gray bar in Fig. 2b) using the MPI-ESM value of the transient response to cumulative emissions.[8]
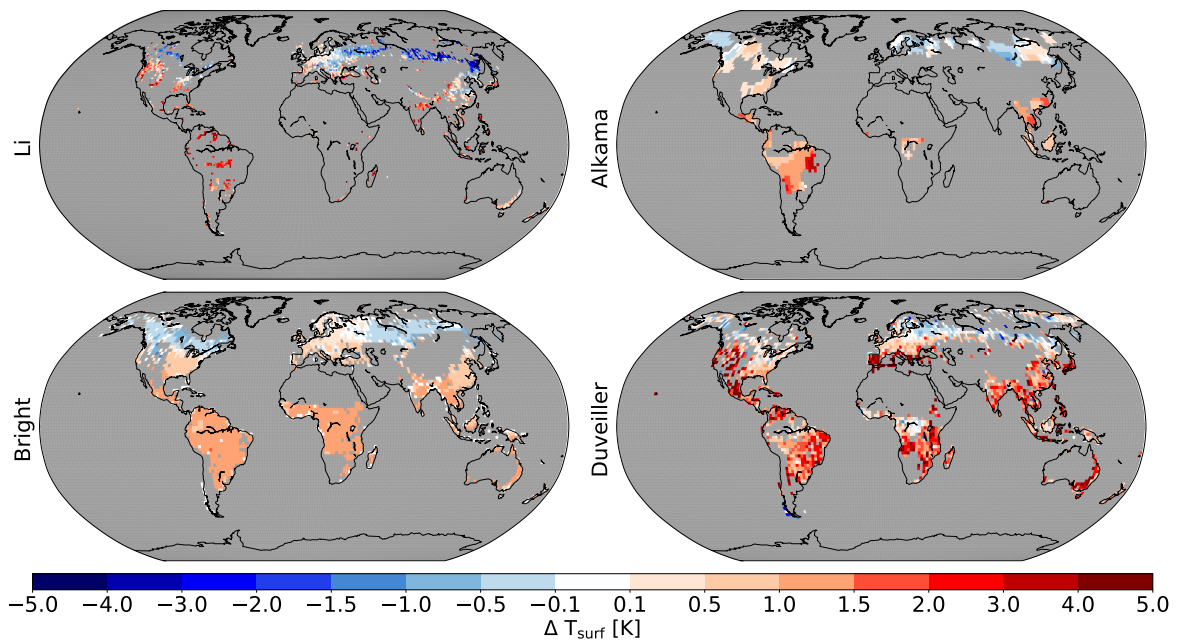


Figure S1: Local effects of deforestation on surface temperature [K] in observation-based datasets. These datasets comprise satellite-based observations on potential (Li et al.[2] and Duveiller et al.[4]) and actual deforestation (Alkama & Cescatti[3]), and a semi-empirical approach based on fluxnet observations (Bright et al.[5]).
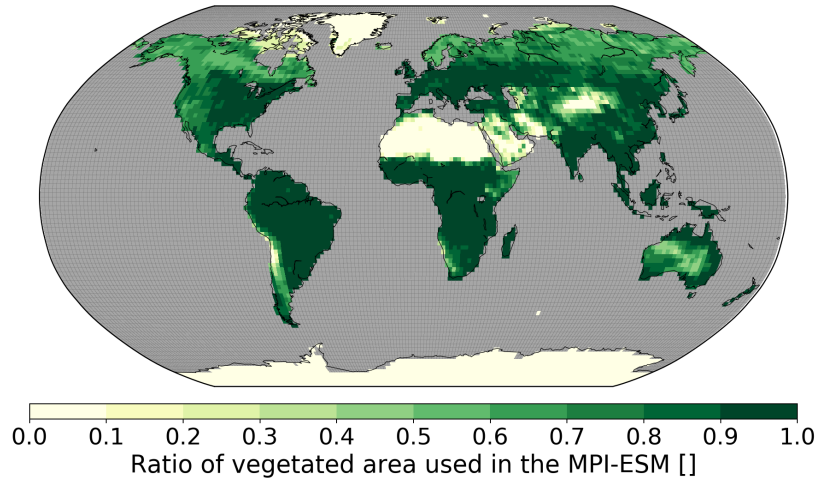
4

Figure S2: Vegetated fraction[9] that we used for the idealized scenarios in the MPI-ESM. We switch between 100% forests and 100% grasslands only on the vegetated parts of the model grid cells. Thus, we simulate no forest cover change in desert areas such as the Sahara.

| Simulation | Short description |
|---|---|
| forest world | Forest prescribed on all vegetated areas |
| 1/4 | Grasses replace forests in 1 out of every 4 grid cells globally |
| 2/4 | Grasses replace forests in 2 out of every 4 grid cells globally |
| 3/4 | Grasses replace forests in 3 out of every 4 grid cells globally |
| low lats | Grasses replace forests in 3 out of every 4 grid cells between $17°$ S and $17°$ N |
| intermediate lats | Grasses replace forests in 3 out of every 4 grid cells between $17°$ and $41°$ S and between $17°$ and $41°$ N |
| high lats | Grasses replace forests in 3 out of every 4 grid cells north of $41°$ N |
| 2x_historical | Grasses replace forests near areas that were deforested since 1850 but, for comparability, with areal extent similar to '1/4' (approximately twice the extent of deforestation since 1850) |
| only albedo | Only albedo switched from forest to grass values in 3 out of every 4 grid cells globally |

Table S1: Overview of all simulations performed for this study. Details can be found in the main text (Methods).
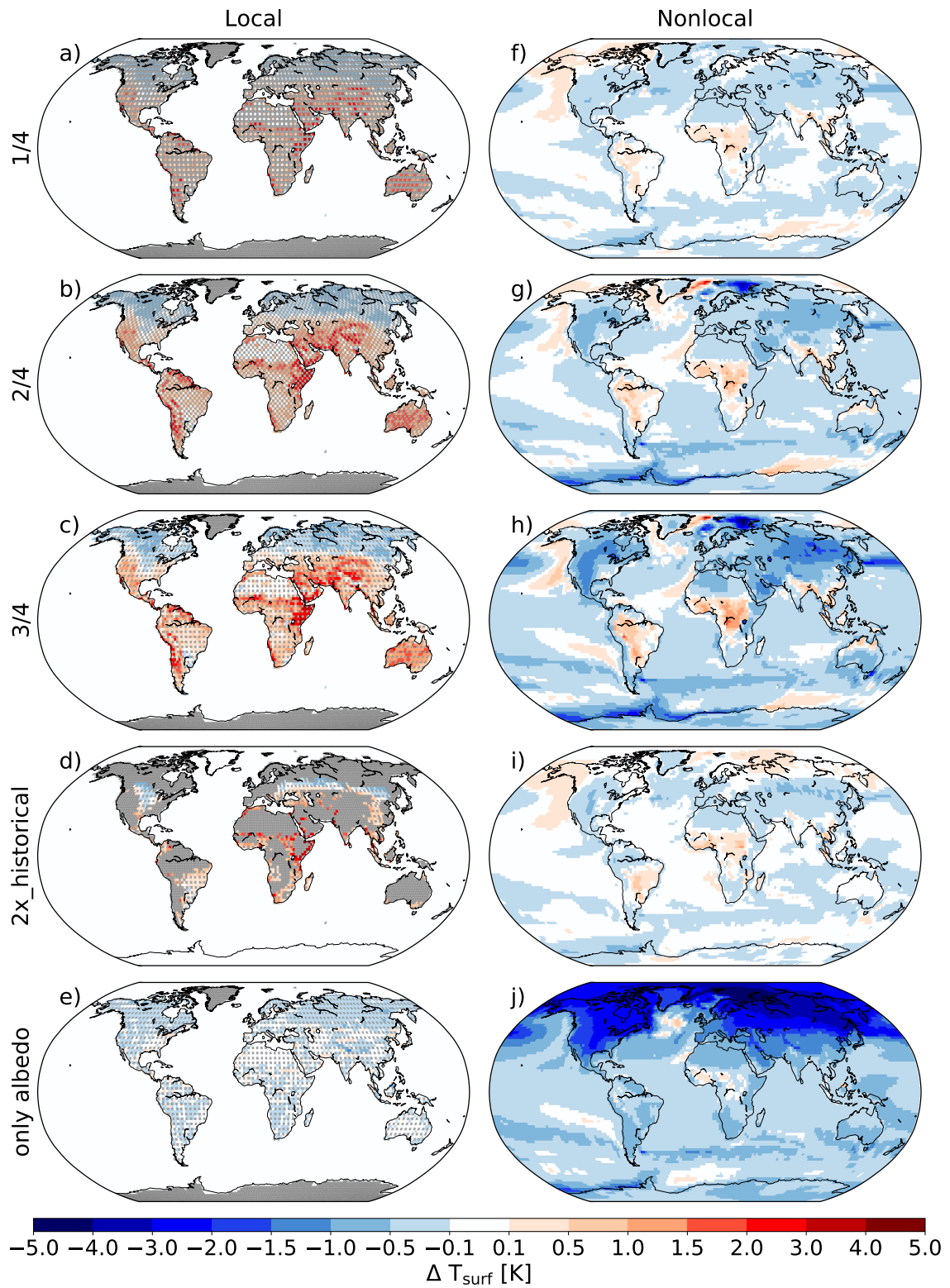
Figure S3: Local and nonlocal effects of deforestation simulated by the MPI-ESM. See Methods section for meaning of simulation names. Shown are changes in surface temperature [K] induced by deforestation (rows 1 - 4) or induced by changes in surface albedo (last row). Land grid cells where vegetation is not changed are masked in gray. It can be seen that local and nonlocal effects of deforestation on surface temperature differ both in the intensity (local effects stronger than nonlocal effects in many grid boxes) and spatial extent (more grid boxes affected by nonlocal than by local effects).
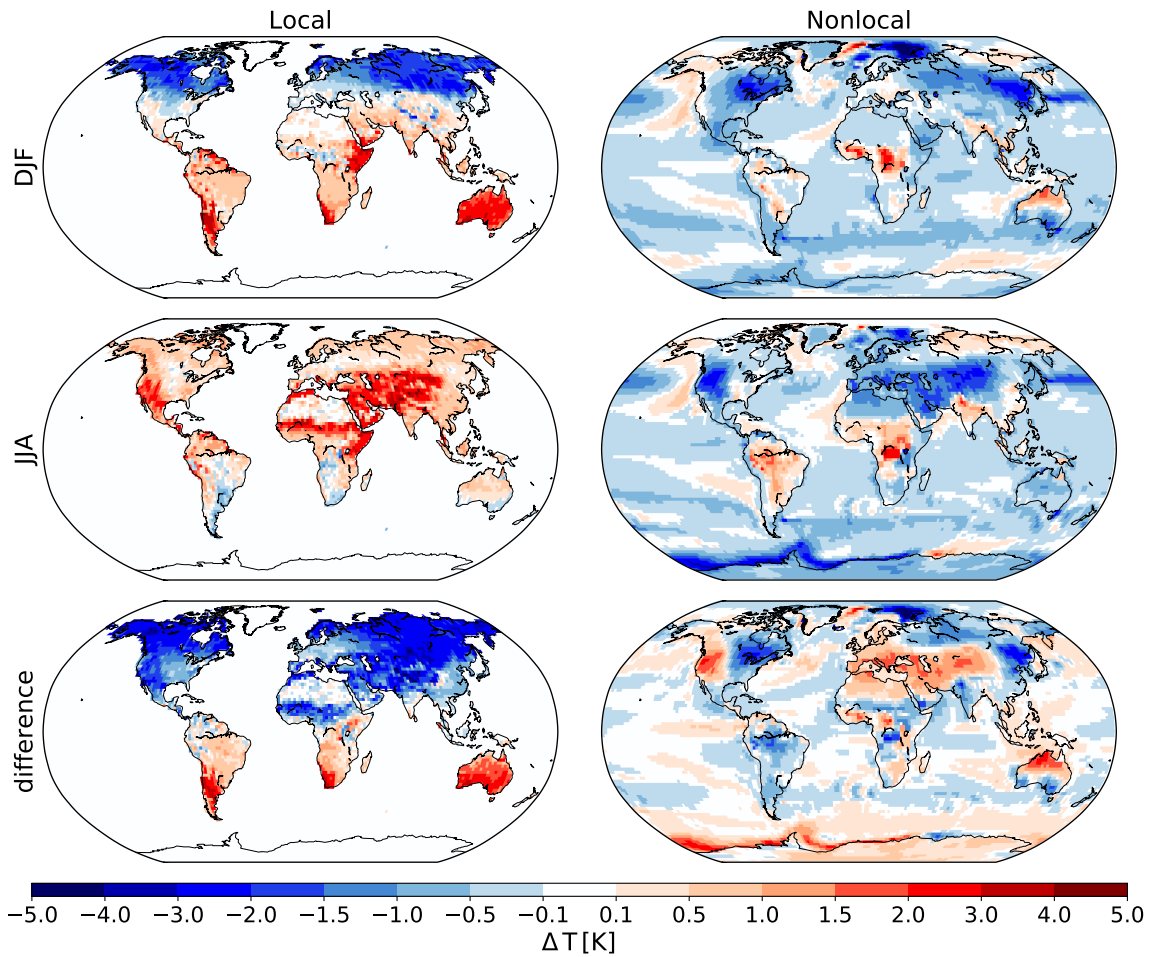
Figure S4: Seasonal values for the nonlocal effects on surface temperature [K] in the MPI-ESM. Changes in surface temperature when simulating deforestation of three of four grid cells globally, in the northern-hemisphere winter (DJF) and summer (JJA) and the difference between the responses in the two seasons (DJF-JJA). Differences between the seasons are particularly pronounced for the local effects, for which deforestation is more cooling/less warming in the northern-hemisphere and more warming/less cooling in the southern hemisphere during DJF compared to JJA. The nonlocal effects on surface temperature seem to vary much less with the season compared to the local effects, with more spatial heterogeneity in the difference between DJF and JJA.
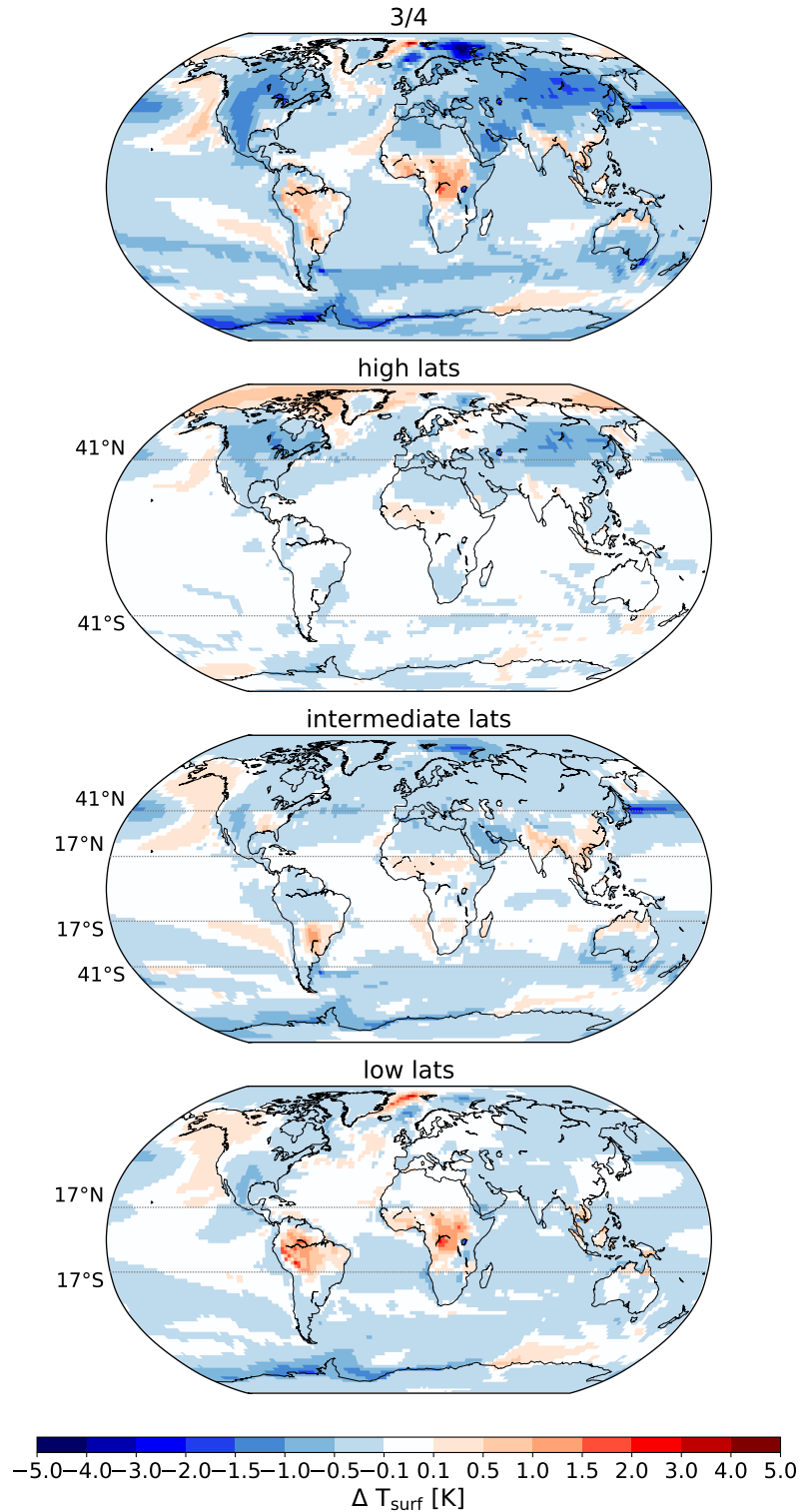
Figure S5: Nonlocal effects on surface temperature [K] in the MPI-ESM and the contributions from deforestation in latitudinal bands. Changes in surface temperature when simulating deforestation of three of four grid cells globally, in the high, intermediate, and low latitudes. The dashed lines denote the borders of deforestation in the respective simulations. Statistical significance of the maps of the simulated (local plus nonlocal) effects is shown in Fig. S9. The global averages of the nonlocal effects shown here are statistically significant for deforestation in each latitude band, see confidence intervals in Fig. 2$b$ in the main text.
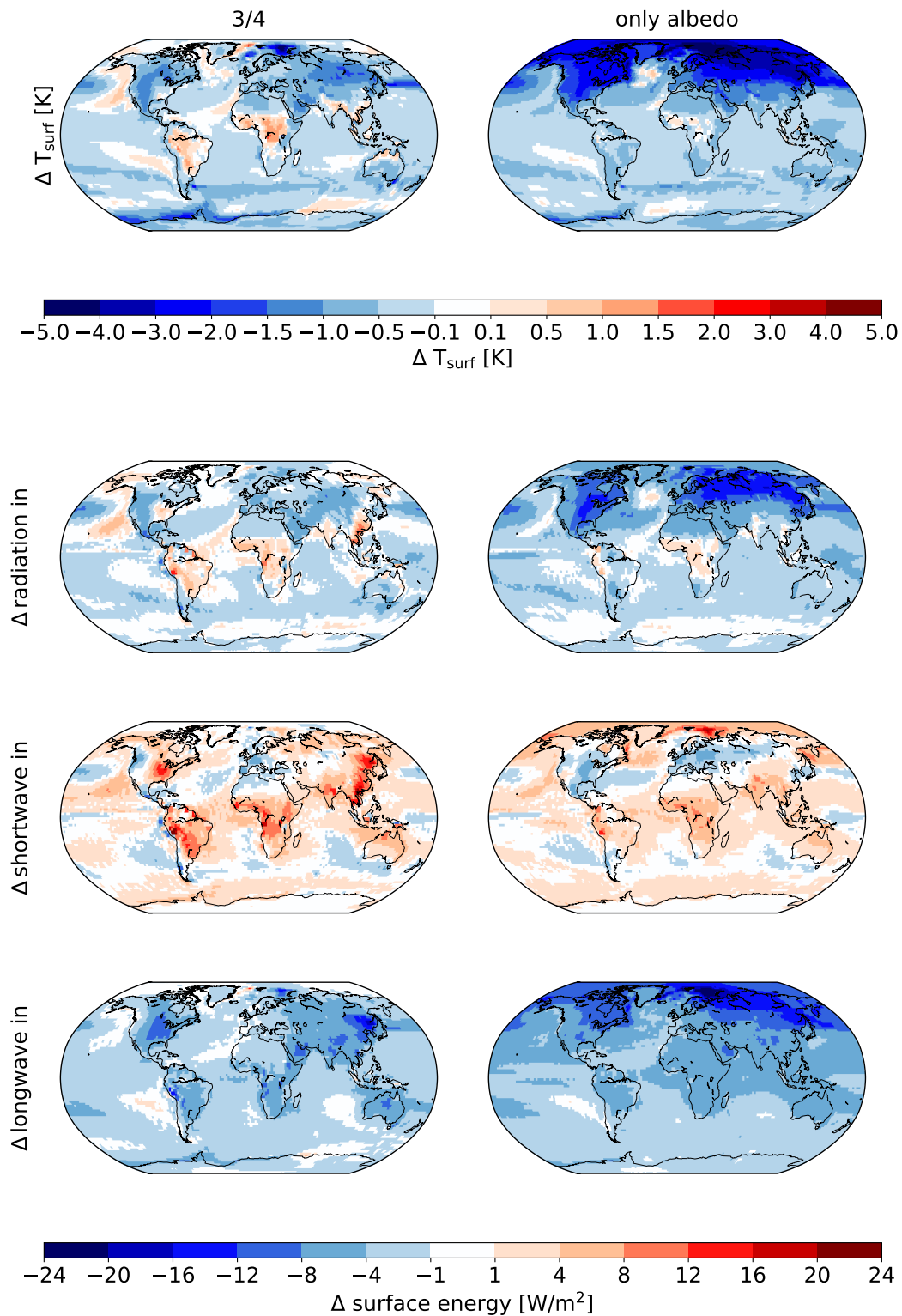
Figure S6: Role of shortwave and longwave incoming radiation for the nonlocal effects as simulated in the MPI-ESM. Left: Nonlocal effects due to deforestation of three out of four grid cells (simulation '3/4', as in Fig. 3 and S3). Right: Nonlocal effects if only albedo is changed from forest to grass values (simulation 'only albedo'). Top: Changes in surface temperature [K]. Bottom: Changes in the total incoming radiation [W/m$^2$], split further into changes in shortwave incoming radiation and longwave incoming radiation.
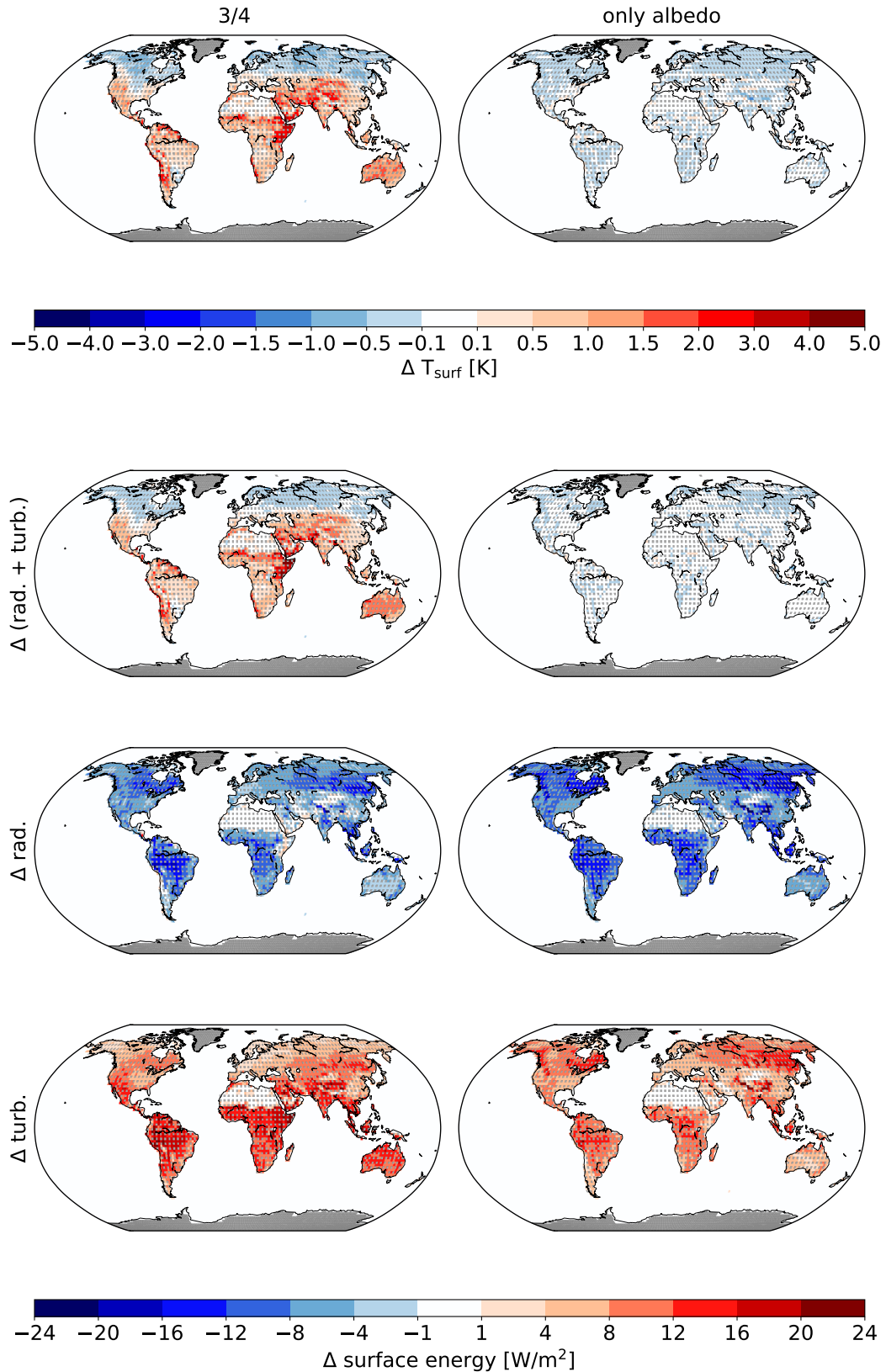
Figure S7: Role of radiation and turbulent heat fluxes for the local effects as simulated in the MPI-ESM. Left: Local effects due to deforestation of three out of four grid cells (simulation '3/4', as in Figs. 1 and S3). Right: Local effects if only albedo is changed from forest to grass values (simulation 'only albedo'). Top: Changes in surface temperature [K]. Bottom: Changes in the energy balance [W/m$^2$], split further into changes in radiation (longwave incoming + shortwave net radiation) and turbulent heat fluxes (latent + sensible heat). Even if only the albedo is changed, the resulting radiative cooling is largely compensated locally by more surface energy that is available because of the decreased turbulent heat fluxes from the surface to the atmosphere.
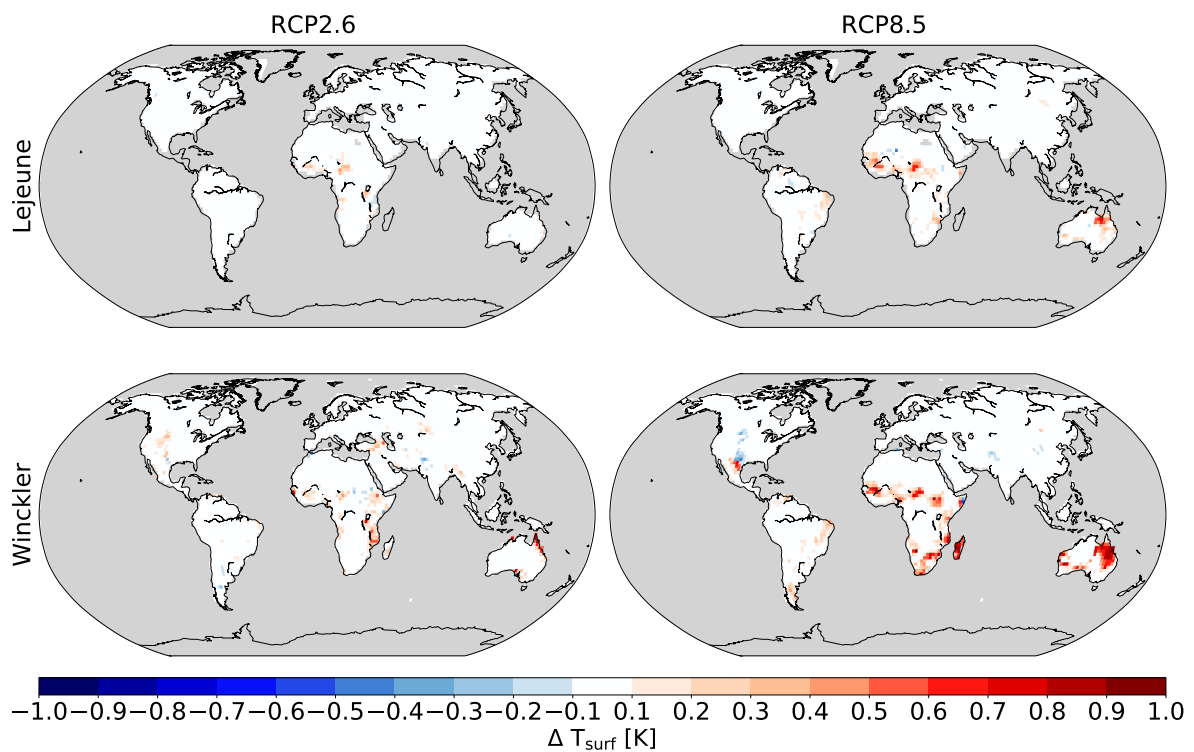
Figure S8: Comparison of the two approaches used in the present study for isolating the local effects on surface temperature [K] in the MPI-ESM. The local effects of RCP2.6 and RCP8.5 are calculated as in the studies by Lejeune et al.[1] and Winckler et al.,[10] respectively. The spatial patterns match well, but the magnitude of the effects differ by a factor of about two. The regression used in the first of the two approaches may lead to an underestimation of the local effects.[1] An underestimated local warming would imply an underestimated nonlocal cooling (or overestimated nonlocal warming), so this underestimation of the local effects does not affect our conclusion that there is a tendency towards nonlocal cooling across the models.
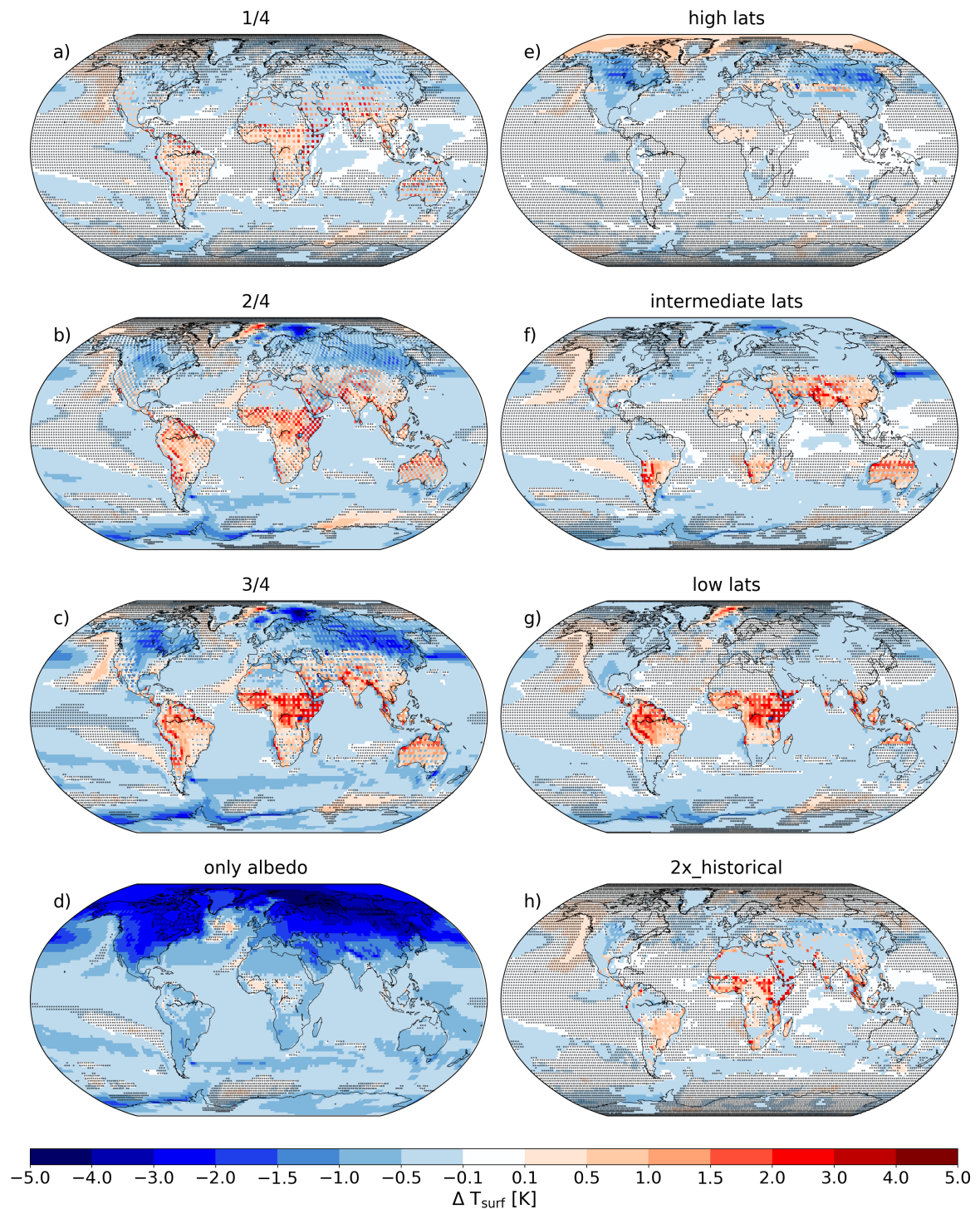
Figure S9: This plot indicates which of the simulated changes in surface temperature (local plus nonlocal) are statistically significant. The simulation names are described in the Methods section of the main text and in Supplementary Table S1. We test for significance using a two-tailed student's t-test accounting for temporal lag-1 autocorrelation.[11] The gray stippling indicates grid boxes where the null hypothesis cannot be rejected and therefore the results are not statistically significant. Panels a)-c) show that the number of statistically significant grid cells increases with the area of forest cover change. When globally averaged, the results both for local and nonlocal effects are statistically robust also in the simulations with smaller deforestation areas (a) and e)-h)) because the 95% confidence interval does not contain zero (Fig. 2 in the main text). This indicates that averaging 200 simulated years is sufficient for the analysis of the global mean values that we perform in the results section in the main text.

Table S2: Overview of simulations used in the inter-model comparison in Fig. 3. For this comparison, simulations with two set-ups were included. In some models, the values for historical land use were obtained from the difference between land use simulations (LU) containing only the land-use forcing ('onlyLU' which is a subset of simulations of 'historialMisc' in CMIP5) and as reference (Ref.) simulations a pre-industrial control run ('piControl' in CMIP5). In another set-up, values were obtained from the difference between all-forcing runs including land use ('historical', 'RCP2.6', and 'RCP8.5' in CMIP5, respectively) and reference simulations that exclude land use ('noLU' which is another subset of 'historicalMisc', 'L2A26', and 'L2A85' respectively). Each value plotted in Fig. 3 is the 30-year mean of the difference between one ensemble member of LU minus one ensemble member of Ref. The numbers in the table denote the number of available ensemble members that were available for the respective model. For instance, for the historical case IPSL-CM5A-LR provides $6 \times 3 = 18$ combinations of ensemble members. The piControl runs are substantially longer than 30 years. Thus to ensure comparability across the two set-ups used for historical land use, we cut 180 years of the control run into 6 'ensemble members', each of which comprises 30 years. Note that the two GFDL models are plotted together as 'GFDL-ESM2' in Fig. 3.

| Set-up | Model | Historical | | | | | | | Future | | | | | | | | |
| | | historical - noLU | | | onlyLU - piControl | | | | RCP2.6 - L2A26 | | | | RCP8.5 - L2A85 | | | | |
| | | IPSL-CM5A-LR | GFDL-ESM2G | GFDL-ESM2M | CESM1-CAM5 | CCSM4 | CanESM2 | HadGEM2-ES | MPI-ESM-LR | MIROC-ESM | CAN-ESM2 | HADGEM2-ES | MPI-ESM-LR | MIROC-ESM | CAN-ESM2 | HADGEM2-ES | IPSL-CM5A-LR |
| LU | | 6 | 1 | 1 | 3 | 3 | 5 | 4 | 3 | 1 | 3 | 4 | 3 | 1 | 3 | 4 | 1 |
| Ref. | | 3 | 2 | 2 | 6 | 6 | 6 | 6 | 2 | 1 | 3 | 4 | 2 | 1 | 3 | 4 | 4 |

# References

[1] Q. Lejeune, E. L. Davin, L. Gudmundsson, J. Winckler, and S. I. Seneviratne, "Historical deforestation increased the risk of heat extremes in northern mid-latitudes," *Nature Climate Change*, vol. 8, pp. 386–390, 2018.

[2] Y. Li, M. Zhao, S. Motesharrei, Q. Mu, E. Kalnay, and S. Li, "Local cooling and warming effects of forests based on satellite observations.," *Nature Communications*, vol. 6, pp. 1–8, 2015.

[3] R. Alkama and A. Cescatti, "Biophysical climate impacts of recent changes in global forest cover," *Science*, vol. 351, pp. 600–604, 2016.

[4] G. Duveiller, J. Hooker, and A. Cescatti, "A dataset mapping the potential biophysical effects of vegetation cover change," *Scientific Data*, vol. 5, pp. 1–15, 2018.

[5] R. M. Bright, E. L. Davin, T. L. O'Halloran, J. Pongratz, K. Zhao, and A. Cescatti, "Local temperature response to land cover and management change driven by non-radiative processes," *Nature Climate Change*, vol. 7, pp. 296–302, 2017.

[6] J. Winckler, C. H. Reick, and J. Pongratz, "Robust identification of local biogeophysical effects of land-cover change in a global climate model," *Journal of Climate*, vol. 30, no. 3, pp. 1159–1176, 2017.

[7] E. Hansis, S. J. Davis, and J. Pongratz, "Relevance of methodological choices for accounting of land use change carbon fluxes," *Global Biogeochem. Cycles*, vol. 29, pp. 1230–1249, 2015.

[8] N. P. Gillett, V. K. Arora, D. Matthews, and M. R. Allen, "Constraining the ratio of global warming to cumulative $CO_2$ emissions using CMIP5 simulations," *Journal of Climate*, vol. 26, pp. 6844–6858, 2013.

[9] C. H. Reick, T. Raddatz, V. Brovkin, and V. Gayler, "Representation of natural and anthropogenic land cover change in MPI-ESM," *Journal of Advances in Modeling Earth Systems*, vol. 5, pp. 459–482, 2013.

[10] J. Winckler, C. H. Reick, and J. Pongratz, "Why does the locally induced temperature response to land cover change differ across scenarios?," *Geophysical Research Letters*, vol. 44, pp. 3833–3840, 2017.

[11] F. W. Zwiers and H. von Storch, "Taking serial correlation into account in tests of the mean," *Journal of Climate*, vol. 8, no. 2, pp. 336–351, 1995.